Nanoscale

PAPER

View Article Online
View Journal | View Issue

Cite this: *Nanoscale*, 2014, **6**, 4250

Controlled assembly of layer-by-layer stacking continuous graphene oxide films and their application for actively modulated field electron emission cathodes

Yuan Huang, Juncong She,* Wenjie Yang, Shaozhi Deng and Ningsheng Xu

A featured "vapor transportation" assembly technique was developed to attain layer-by-layer stacking continuous graphene oxide (GO) films on both flat and concavo-concave surfaces. Few-layer (layer number < 10) GO sheets were "evaporated" (carried by water vapor) from the water-dispersed GO suspension and smoothly/uniformly tiled on the substrate surface. We have found evidence of the influence of the deposition time and substrate–liquid separation on the film thickness. A model was proposed for interpreting the assembly process. It was found that a current conditioning would induce a reduction of the GO surface and form an Ohmic contact between the GO–metal interfaces. Accordingly, an actively modulated GO cold cathode was fabricated by locally depositing continuous GO sheets on the drain electrode of a metal-oxide-semiconductor field effect transistor (MOSFET). The field emission current of the GO cathode can be precisely controlled by the MOSFET gate voltage (V_{GS}). A current modulation range from 1×10^{-10} A to 6.9×10^{-6} A (4 orders of magnitude) was achieved by tuning the V_{GS} from 0.812 V to 1.728 V. Due to the self-acting positive feedback of the MOSFET, the emission current fluctuation was dramatically reduced from 57.4% (non-control) to 3.4% (controlled). Furthermore, the integrated GO cathode was employed for a lab-prototype display pixel application demonstrating the active modulation of the phosphor luminance, *i.e.* from 0.01 cd m^{-2} to 34.18 cd m^{-2}.

Received 22nd September 2013
Accepted 17th January 2014

DOI: 10.1039/c3nr05058k

www.rsc.org/nanoscale

1. Introduction

Graphene-based materials have attracted intensive attention for micro/nano-electronic applications. Among them, graphene oxide (GO) has showed great potential for applications in transparent electrode,[1] field effect transistor[2] and field electron emission cathode.[3] The progresses on the synthesis of reduced GO by chemical exfoliation[4] open up a possibility for developing up-scalable graphene-based field emission cathodes. For example, Koh *et al.* prepared reduced GO field emitters by electrophoretic deposition and the films showed low field electron emission, *i.e.* 10 μA cm^{-2} at 0.68 MV m^{-1}.[5] Ye *et al.* prepared reduced GO sheets supported on nanometer-scale sharp Ni nanotip arrays offering an emission current of 1 μA at 0.5 MV m^{-1}.[6] The works show that the reduced GO is a promising cathode material for vacuum electronic applications. However, there are challenges for attaining high performance GO cathodes. It has been reported that electrons may emit from the sharp edges of the GO (ref. 7) and the electronic structure of the edge significantly affects the electron tunneling probability.[8] Thus, small variations in emitter geometrical or electrical structures would result in a considerable variation in emission properties. Additionally, the presence of oxygen functional groups and defects also showed a significant effect on current stability and uniformity of the GO cathode.[9] It limits the application of GO in vacuum electronic devices. Furthermore, accurate control of the field emission current is an important feasibility requirement for field emission cathodes. The common approach is to fabricate an integrated extraction gate with the cathode to form a triode structure.[10] However, so far, limited efforts have been devoted to the integration of triode GO devices due to the lack of well-controlled methods for GO assembly.

The connection of the cathode in series with a ballast resistor or a field effect transistor (FET) is one of the effective solutions to improve the emission current stability and spatial uniformity as well as to precisely control the emission current.[11–14] Both the ballast resistor and the FET have a noise buffer effect, while the connection with a FET possesses an additional advantage, *i.e.* the emission current can be precisely modulated by tuning the FET gate voltage.[13,14] This makes it possible to drive the cathode by a commercial integrated circuit. However, graphene prepared by chemical vapor deposition[15] or SiC epitaxial

State Key Laboratory of Optoelectronic Materials and Technologies, Guangdong Province Key Laboratory of Display Material and Technology, School of Physics and Engineering, Sun Yat-sen University, Guangzhou 510275, People's Republic of China. E-mail: shejc@mail.sysu.edu.cn

growth[16] involves high temperature processes, which is far beyond the endurance of the traditional FET devices. For GO, derived from chemical oxidation methods,[4] the key challenges associated with its incorporation into FET-modulated devices are (i) effective and controllable methods for assembling uniform GO films; (ii) efficient reduction of GO for the improvement of conductivity and field emission properties. To address these issues, we have developed, and report herein, a "vapor transportation" transfer method for achieving layer-by-layer stacking continuous GO films from a GO suspension. Actively modulated GO cold cathodes were demonstrated by locally depositing GO films on the drain electrode of a metal-oxide-semiconductor field effect transistor (MOSFET). A lab-prototype display pixel application by employing the integrated GO cathode was demonstrated. The work not only opens up a new avenue for achieving layer-by-layer stacking continuous GO films, but also is meaningful to the applications of actively-controlled GO cold cathodes for vacuum electronic devices.

2. Experimental

The GO was prepared using the Hummers method[17] and dispersed in deionized water by ultrasonication for 5 hours to obtain a yellow-brown GO suspension (1 mg mL^{-1}). The layer number of the GO sheets in the suspension is typically less than 10.[9] The featured technique for the present work is the transfer of the few-layer GO sheets from the suspension to the substrate, forming a continuous film. Si substrate of an area of 1×1 cm^2 was used. As indicated in Fig. 1a, the substrate was put upside-down above the GO suspension and placed on the center of the container. The substrate surface was parallel to the liquid level. There is no contact between the sample and the container side-wall. Subsequently, the solution was heated in an oil bath at 100 °C with a water-cooled condenser. The sample was separated from the water-cooled condenser by ~17.5 cm. Along with the evaporation, the sample surface was coated with a thin GO film. The transfer process described above is denoted as "vapor transportation deposition" (VTD) in the following discussion. An integrated MOSFET-GO cathode was fabricated by locally depositing GO films on the drain electrode of a MOSFET. A commercially available N-channel enhancement MOSFET (Infineon: BSP 324) was used. The use of the "Infineon: BSP 324" MOSFET is due to its relatively high maximum-rating drain–source voltage (400 V), lower in both the zero-gate-voltage drain current (10 nA) and gate-source leakage current (10 nA). These characteristics are advantageous for enhancing the reliability of the integrated MOSFET-controlled GO cathode. Firstly, a buffer layer of Cr (200 nm) was locally deposited on the drain electrode of the MOSFET by using ultraviolet photolithography and sputtering techniques. Secondly, a thin film of few-layer GO was deposited on the Cr surface employing the VTD. The deposition time is 2 hours and the separation between the substrate surface and the liquid level is 2.0 mm. Finally, a lift-off process was employed to remove the photoresist (RZJ4810) and leave the defined GO pattern.

The surface morphology and structure of the GO film was analyzed by scanning electron microscopy (SEM; ZEISS Supra 55), atomic force microscopy (AFM; CSPM5500) and high resolution transmission electron microscopy (HRTEM; JEM-2010). X-ray photoelectron spectroscopy (XPS; Thermo Fisher Scientific ESCALAB 250) was used to investigate the elemental composition of the GO surface. The XPS measurements were carried out in an ultra-high vacuum (~2×10^{-7} Pa) with a monochromatic Al Kα radiation source. The binding energy

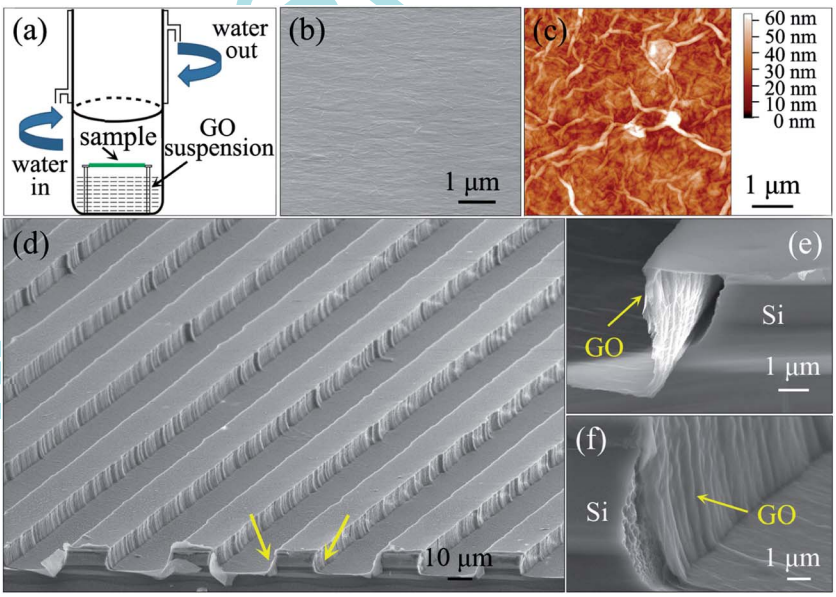

Fig. 1 (a) A schematic illustration shows the arrangement of the sample, GO suspension and water-cooled condenser for GO transfer. (b) and (c) are the typical SEM (75°-tilted) and AFM images of the GO film on a smooth Si substrate, respectively. (d) The typical cross-sectional SEM image of a GO film deposited on a concavo-concave surface (Si micro-groove). (e) and (f) are the enlarged SEM images of the "left" and "right" arrow-indicated areas shown in (d), respectively.

scale of the instrument was calibrated using the C1s peak (284.8 eV). The two-terminal contact electrical measurements of the GO films were performed in a SEM chamber ($\sim 5 \times 10^{-3}$ Pa) equipped with a nano-manipulated gold-coated tungsten tip probe (~100 nm in radius). A picoammeter with a power supply (Keithley 6487) was employed to record the current. Field emission studies were carried out in a high vacuum chamber ($\sim 2.0 \times 10^{-4}$ Pa) at room temperature. A stainless steel probe (1 mm in diameter) with smooth flat end was used as an anode, with a cathode–anode separation of 100 μm. In the MOSFET actively modulated measurements, a green phosphorous screen was employed as an anode and the cathode–anode separation was kept at 50 μm.

3. Results and discussion

3.1 GO Deposition

In the VTD transfer of GO, it took ~15 minutes for the suspension to reach a stable temperature of 100 °C, while an enrichment collection of GO nano-sheets was formed at the air–water interface. No obvious boiling phenomenon was observed during the whole process. The substrate and the liquid level were well separated. It is believed that the enrichment of the GO layer on the suspension surface[18] decreases the vapor pressure of the GO suspension. Fig. 1b and c give the typical SEM and AFM images of the GO films on a smooth Si substrate. The films were obtained by placing the Si chip 2.0 mm above the liquid level and the deposition time is 2 hours. As indicated in Fig. 1b, the film is continuous and covered the whole surface of the Si substrate, exhibiting wrinkled surface structures. Quasi-one-dimensional creases with a length of ~1 μm and a height of several tens of nanometers were observed with AFM (Fig. 1c). The mean roughness (RMS) on the surface of the GO films is 8.63 nm. Additionally, the films were also deposited on the concavo-concave Si surface (*i.e.* with micro-grooves) by using the same deposition conditions. The Si chip was dissected for obtaining the cross-sectional SEM images (Fig. 1d–f). Fig. 1e and f are the enlarged images from a micro-groove indicated by arrows in Fig. 1d. It is clearly indicated that the film continuously covered the concavo-concave surface. The film thickness across the chip is rather uniform as measured from the SEM image, *i.e.* around ~100 nm. It demonstrated that the VTD method can be employed to achieve continuous GO films on both the smooth and concavo-concave surfaces.

We have found evidence of the deposition time and substrate–liquid separation dependence on the film thickness. Fig. 2a–c give the typical SEM images of the GO films with thickness of ~28 nm, 1.248 and ~2.298 μm, respectively. The films were obtained by fixing the substrate–liquid separation at 2.0 mm and changing the deposition time, *i.e.* 1, 3 and 4 hours. It was found that the thickness, the deposition rate and the surface roughness of the GO films distinctly increased with the prolonging of the deposition time. Furthermore, a decrease in film thickness was observed when the substrate–liquid separation was broadened. In 5 hours deposition, films with thickness of ~20 nm, 1.596 and ~3.617 μm (Fig. 2d–f) were obtained at a substrate–liquid separation of 5.2, 4.2 and 2.0 mm, respectively. For the ultra-thin GO films (*i.e.* 20 and 28 nm), they are well attached to the substrate surface and the cross-sectional views can only show a portion of the films (Fig. 2a and d). In Fig. 2a–f, it is clearly indicated that the continuous GO films are layer-by-layer stacked. However, non-continuous sheets are observed if the deposition time is too short, *i.e.* 5 minutes at a substrate–liquid separation of 2.0 mm. It is worth mentioning that the continuous GO films show strong adhesion to the substrate even after undergoing an ultrasonication. We have performed TEM investigations on the GO sheets covered on a copper grid. The GO sheets were obtained by 5 minutes deposition at a substrate–liquid separation of 2.0 mm. Some individual sheets were observed (Fig. 2g). Except for the overlapped segments, the typical thickness of the individual sheets is 1–4 nm (Fig. 2h), formed by several layers (<10 layers) of GO. The TEM evidence suggests that only few-layer GO sheets were transferred to form the continuous film.

The following discussions are mainly focused on how the GO sheets were "evaporated" and tiled on the surface. In the VTD, bubbles were generated because of the decrease of air solubility in the heated GO suspension. The GO sheet is composed of a largely hydrophobic basal plane with hydrophilic edge; it would adhere to the rising bubbles and become thermodynamically trapped after they reach the air–water interface to minimize the surface energy (*i.e.* lower the surface tension).[18] The air solubility did not change further when the temperature stabilized at 100 °C. We believed that most of the bubbles were generated during the increase of the suspension temperature, *i.e.* within 15 minutes. The bubble "breaking" at the air–water interface may induce a splashing of the GO flakes, which is one of the ways to "transfer" the GO sheets. With the prolonging of the heating time, few air bubbles appeared while upward convection flows induced by heating accelerated the surface enrichment of GO sheets.[18] The enrichment collection of GO sheets at the air–water interface can block the splashing of the GO flakes. Therefore, it is reasonable to propose that the splashing of GO flakes in the bubble "breaking" only happened at the very beginning of the heating.

According to kinetic theory, the average kinetic energy per water molecule can be derived by $E = 6/2\ kT = 3\ kT$, where $k = 1.3806488 \times 10^{-23}$ J K^{-1} and T is the thermodynamic temperature (in K). An average kinetic energy per water molecule value of 1.545×10^{-20} J (*i.e.* 96.43 meV) was obtained when $T = 373.15$ K. Since the collected few-layer GO sheets at the air–water interface were attracted to each other through van der Waals forces,[19,20] the interaction energy between the few-layer GO sheets is about 60–97 meV.[21–23] Accordingly, it is reasonable to speculate that the GO sheets were peeled-off from the air–water interface by large numbers of water molecules (Fig. 2i). The peeled-off few-layer GO sheets were transferred toward the substrate surface by the water vapor stream. Some of the GO sheets may tile on the substrate by van der Waals attraction, while others may attach on the surface of the water droplets which were formed by the condensed vapor (Fig. 2j). We believed that the water condensation was not due to the cooling effect as the sample was separated from the water-cooled condenser by ~17.5 cm. The high vapor pressure in the substrate–liquid gap was taken into account. Unfortunately, the substrate–liquid gap is too narrow (2–5 mm) to make a direct

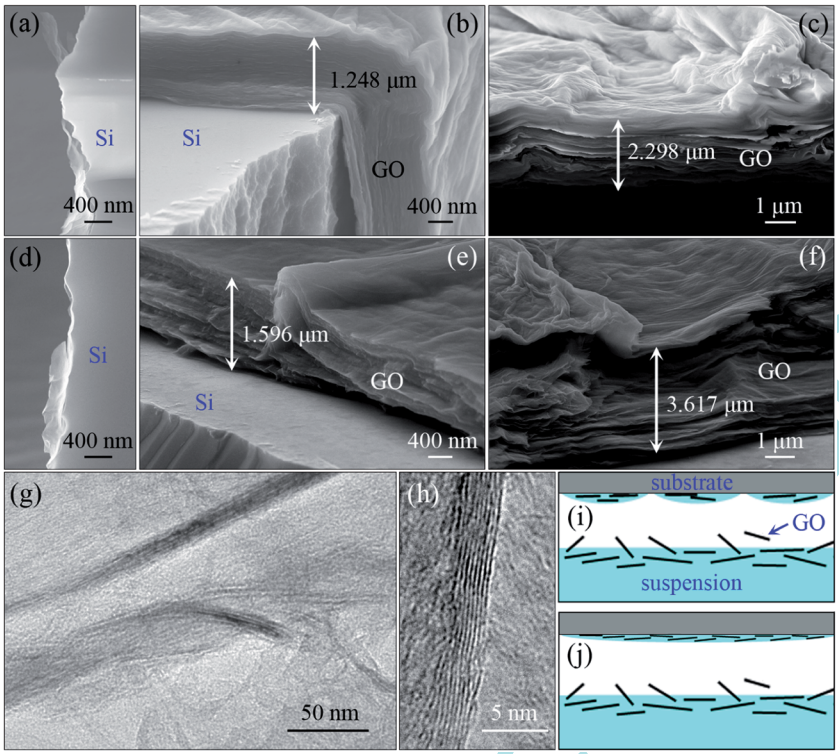

Fig. 2 (a–c) The typical SEM images of the GO films obtained by 1, 3 and 4 hours deposition, respectively. The substrate–liquid separation is 2.0 mm. (d–f) The typical SEM images of the GO films obtained by fixing the substrate–liquid separation as 5.2, 4.2 and 2.0 mm, respectively. The deposition time is 5 hours. (g) and (h) The typical TEM images of the GO sheets covered on a copper grid which was obtained by 5 minutes deposition at a substrate–liquid separation of 2.0 mm. (i) and (j) The schematic illustration for the VTD process.

observation of the water condensation. The GO sheets may pile up in the air–water interface of the droplet due to the effect of hydrophobicity as well as the interface tension.[18] The functional groups at the edge and basal plane of the GO sheets, such as hydroxyl (–OH) and carboxyl (–COOH) groups,[19] can interact with H^+ from the ionized water molecule to form hydrogen bonds. It encouraged the GO sheets to re-disperse in the water droplet. The vapor pressure can drive the droplets to drift along the substrate surface, while the van der Waals force, the π–π bonds between the adjacent GO sheets and the hydrogen bonds promote the self-assembly of the GO stacked structure. The drifting of the water droplet is advantageous for the GO sheets to diffuse from the high concentration area to the low concentration one. The diffusion improves the uniformity of the film. Meanwhile, some droplets were reunited and fell back to the suspension under gravity. Based on the above discussion, we proposed the following for the correlation between the deposition rate (also the surface roughness) and the deposition time. At the beginning of the deposition, water droplets had difficulty drifting along the substrate surface due to the hydrophobicity of Si. Accordingly, non-continuous films were observed at the initial stage of the deposition. Once the GO sheets were attached to the substrate, it enhanced the hydrophilicity of the surface. Consequently, more GO sheets were attached and the deposition rate was improved. The surface roughness was increased when the GO sheets acquired wrinkles. The rough surface of the GO sheets can further promote the deposition.

As compared to the early reported transfer techniques for graphene-based materials,[24] VTD provides several advantages. First, the thickness of the GO films was controlled over a range of 20 nm to 3.6 μm by adjusting either the deposition time or the substrate–liquid separation. Due to a fact that the deposition process is rather complicated, not only do the deposition time and liquid–substrate separation have significant effect on the thickness of the films, but also the temperature, the concentration of the GO suspension and the numbers of the bubbles. Obviously, these parameters of the vapor transportation deposition need further studies. Second, in our experiment, we found that only few-layer GO sheets were transferred and assembled. This profits from the self-filtered effect of the vapor transportation. Much higher kinetic energy is needed to "evaporate" impurities such as aggregated GO sheets with heavy weights. A "low" evaporated temperature of 100 °C may not provide enough energy to lift them up to the substrate. Third, the GO sheets can be deposited on a concavo-concave surface and form layer-by-layer stacking continuous GO films. No surfactant is needed to improve the adhesion between the GO sheets and the substrate. Final, the VTD is operated at around 100 °C, which is in the endurance temperature range of traditional semiconductor devices (*i.e.* MOSFET), suggesting a potential application for device integration. In the following, we will present the application of the VTD deposited GO films for an actively modulated field emission cathode.

3.2 Improvement of electrical properties

In the field emission of the GO cathode, electrons flowed through the GO–substrate interface, bulk-GO, and GO-vacuum potential barrier in sequence. Therefore, improvements of the GO–substrate electrical contact and conductivity should enhance the emission.[9] We have found that current conditioning is an effective way to attain the above properties. Fig. 3a and b gives the typical *I–V* curves for a two-terminal contact electrical test on a film with 100 nm thickness. It is clearly indicated that to obtain the same current, less applied voltage is needed following the progress of the tests. This suggests an improvement of the conductivity and GO–substrate electrical contact. Typically, 9 test cycles were needed to achieve reproducible *I–V* curves (curves 10–13 in Fig. 3a). The straight-line behavior of curves 12 and 13 (Fig. 3b) suggested the forming of an Ohmic contact. No morphology change of the GO film was observed after the test with the maximum current of 0.266 μA. We compared the equivalent resistance of the GO films derived from the linear section of the *I–V* curves. Resistance values of 1.41×10^8 Ω and 1.14×10^6 Ω were obtained from curve 1 and curve 13, respectively. The resistance was decreased by two orders of magnitude. According to Wei *et al.*,[25] local thermo-conditioning can cause a reduction of GO and improve the conductivity by four orders of magnitude. It is reasonable to propose that the conductivity of the GO films increased due to the *in situ* reduction which is induced by the Joule heating effect of the current. Considering that the GO films studied in the present work are layer-by-layer stacking GO sheets, the current may transfer between inter layers. It has been reported that Joule heat can also induce a change of open-end multilayered graphenes into closed ones.[26] Thus, in our work, the structural change of the layer-by-layer stacking GO sheets under the current conditioning is presumably induced by Joule heat. The edge of the GO sheets may connect and offer more pathways for electron transportation.

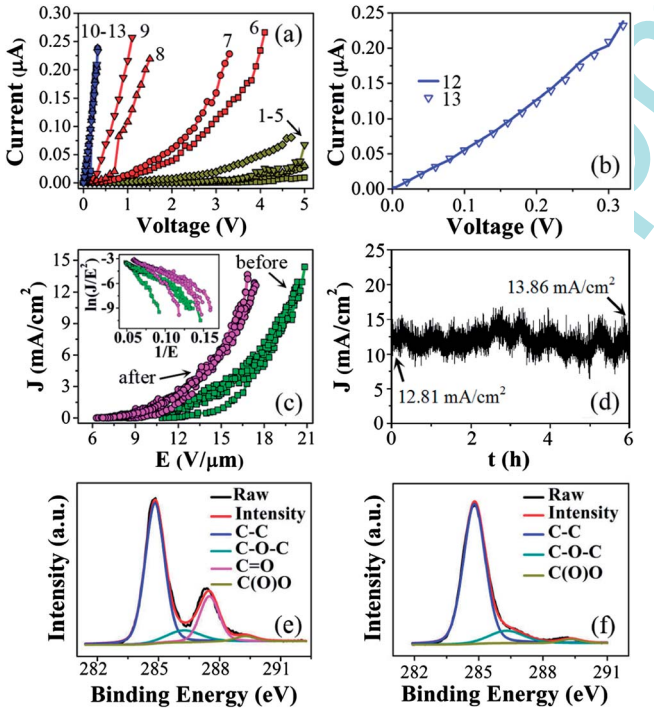

Fig. 3 (a) and (b) The *I–V* characteristics of the GO film obtained by the two-terminal conductance tests. The inset numbers in (b) represent the "cycle number" of the test. (c) The typical *J–E* curves and the corresponding F–N plots for the samples before and after 6 hours of field emission current conditioning. (d) The typical *J–t* curves during the field emission current conditioning. (e) and (f) The typical XPS spectra of the GO cathode surface before and after 6 hours field emission current conditioning.

We performed XPS measurements on the GO film which has experienced the two-terminal conductance tests. The minimum light spot area of the XPS instrument is $\sim 2 \times 10^5$ μm^2. The X-ray spot was adjusted to cover the probe–GO contact area (typically $\sim 3.14 \times 10^{-2}$ μm^2). No evidence was obtained indicating a reduction of the film. The result is reasonable, since the probe–GO contact area is rather small as compared to that of the X-ray spot. The signals were mainly from the non-contact area. This result strongly suggested that no reduction occurred on the films around the probe–GO contact position.

We further extended the current *in situ* reduction method by employing a field electron emission current with a stainless steel probe. In Fig. 3c, the green (with square symbols) curves show the typical field emission current density *vs.* electric field (*J–E*) and the corresponding Fowler-Nordheim (F–N) plots of the GO films before the conditioning. The turn-on field (E_{to}, with current density of 10 μA cm^{-2}) and threshold field (E_{th}, with current density of 10 mA cm^{-2}) are 7.6 MV m^{-1} and 19.7 MV m^{-1}, respectively. Then, we performed the conditioning by running the cathode for 6 hours with a starting current density of 12.81 mA cm^{-2} (Fig. 3d). Afterward, the field emission *J–E* properties were re-tested and were given in Fig. 3c as the purple curves (with cycle symbols). It showed that the field emission was enhanced after the conditioning. The turn-on and threshold fields were reduced to 6.7 MV m^{-1} and 16.5 MV m^{-1}, respectively. The water desorption from the GO cathode may be one of the possible reasons for the enhanced field emission.[27] The elemental composition of the GO before and after current conditioning was investigated by XPS (Fig. 3e and f). By fitting the spectra as the convolution of a Gaussian and Lorentzian function, four oxidation components that correspond to carbon atoms in different functional groups were observed: C–C (284.8 eV), C–O–C (286.3 eV), C═O (287.5 eV), O–C═O (289.3 eV). It was found that the atomic ratio of carbon and oxygen (C/O ratio) of the GO film surface was increased from 2.84 to 5.24 after the conditioning. This implies that *in situ* reduction of the GO surface occurred during the field emission test. The reduction of GO is an effective way to improve the field emission characteristics of the GO. After reduction, C═O bonds and the C–O–C at the armchair edge were broken which resulted in a decrease of the surface potential barrier and thus enhanced the electron emission.[9] In the field emission test, residuals may desorb from both the anode and the cathode and form ions to bombard the surface. The bombardment may be one of the reasons for inducing desorption of the C–O–C and C═O groups from the surface. The F–N plots before and after the 6 hours field emission conditioning exhibit the

approximately the same slopes at the high current region, suggesting a resistance-induced saturation. It implies that the field emission conditioning resulted in an increased emission area that is consistent with the reduction of the GO surface as observed by XPS but may not be consistent with the decreased resistance of the bulk GO and GO–substrate interface. The field emission current density (12.81 mA cm^{-2}) is much lower (4 orders of magnitude) than the maximum current density (8.47×10^5 mA cm^{-2}) of the two-terminal electrical measurements. It is reasonable to propose that less Joule heat was generated in the field emission conditioning. Significant reduction may occur at the GO surface with the assistance of electric field force and back ion bombardment while less at the bulk and interface. Therefore, the resistance brings a current saturation in the high emission current region. Nevertheless, the *in situ* reduction of GO by field emission is an effective means to achieve reduced-GO and enhance the field emission. It can avoid the employment of high temperature thermal annealing[1] and toxic reducing agents,[4] showing a promising potential for integrated devices applications.

3.3 Actively modulated GO cathode

The controlled assembly of layer-by-layer stacking continuous GO film was employed to fabricate actively modulated field electron emission cathodes. The fabrication procedures were presented in the Experimental section. A current conditioning for GO reduction was carried out before the modulated test. The source, gate and drain electrodes of the MOSFET were short-circuited and connected to the ground. The anode voltage (V_A) was increased manually in steps of 1 V until an emission current of 6.5 μA was obtained. The emission current was fixed at 6.5 μA for 8 hours by modulating the anode voltage between 730 and 850 V. According to our earlier study, a vacuum breakdown from the zinc oxide nanowires (ZnO-NWs) cathode may result in a high risk of causing a MOSFET failure during conditioning.[14] However, few breakdown issues were induced from the GO cathode in this study. We take the ballast resistor effect and the effective heat dissipation of the layer-by-layer stacking GO into account as the reasons for this observation.

The active-control on the field emission current from the GO film was investigated. Fig. 4a shows the measurement circuit. In Fig. 4b, the emission current (I) is plotted as a function of V_A at various MOSFET gate voltages (V_{GS}). It is clearly seen that the emission current was fixed at a saturation current of the MOSFET at a specific V_{GS} in the high V_A region. Take curve-7 as an example; the emission current was fixed at ~1.05 μA when the V_{GS} was 1.590 V. In this V_{GS}-controlled region, the electron supply to the GO emitter was limited by the MOSFET. The emission current was rather stable for the noise-buffer effect of the MOSFET channel resistance. The F–N equation[28] was used to analyze the field emission behavior of the integrated GO cathode. Fig. 4c indicated the corresponding F–N plots of the I–V_A data shown in Fig. 4b. The F–N plots are divided into two district sections. The slopes of the F–N plots turn to slightly positive in the V_{GS}-controlled region, indicating that the electron supply is limited by the MOSFET. From the F–N plots, we

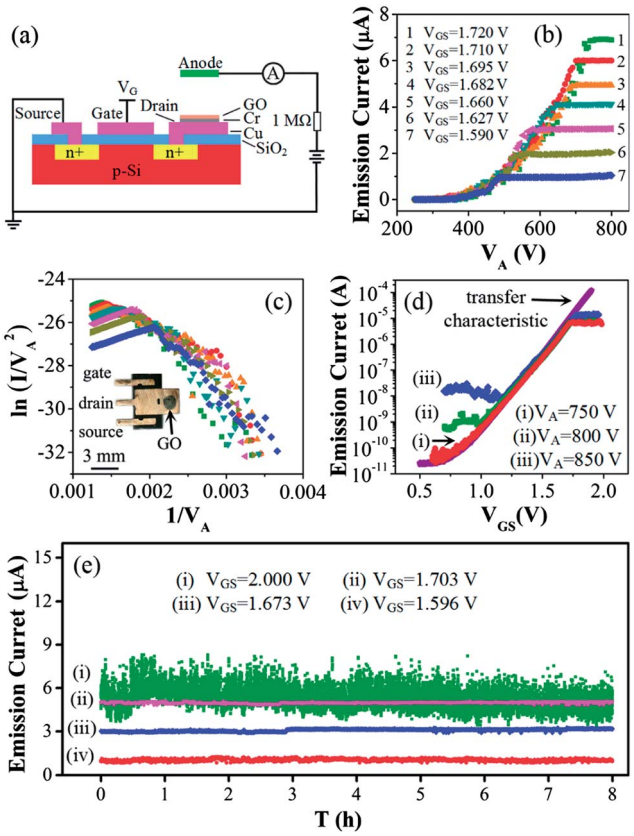

Fig. 4 (a) Schematic of the measurement circuit. (b) and (c) are the typical field emission I–V_A curves and the corresponding F–N plots of the MOSFET-modulated GO cathode, respectively. The inset in (c) is the photograph of the integrated cathode. (d) The typical I–V_{GS} characteristic curves of the integrated GO cathode at various V_A. The transfer characteristic of a pristine MOSFET was also presented. (e) The typical I–t plots of the MOSFET-controlled GO cathode.

can confirm that the field emission current is effectively modulated by the MOSFET.

The correlation between the V_A and the MOSFET-modulated characteristics was further investigated. Fig. 4d shows the I–V_{GS} curves obtained at an anode bias of 750, 800 and 850 V, respectively. The transfer characteristic of a pristine MOSFET obtained at a drain–source bias (V_{DS}) of 10 V was also presented. It was found that the I–V_{GS} curves obtained at a V_A of 750 V

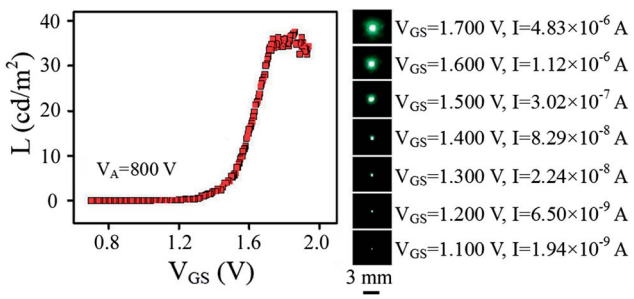

Fig. 5 The typical luminance *vs.* V_{GS} curve and the corresponding images of the display pixel.

coincide with the transfer characteristic of the MOSFET with the leakage current (I_{off}) of ~0.3 nA, indicating that the MOSFET was well protected from the high anode bias. However, a remarkable increase in the leakage current was observed at a V_A of 800 V (I_{off} = ~1 nA) and 850 V (I_{off} = ~10 nA). This is because the MOSFET was operated close to the breakdown region and a higher V_A (thus V_{DS}) resulted in a high leakage current. This finding suggests that a low anode bias voltage is extremely important in the MOSFET-modulated strategy, even though the field emission current can be modulated by a low MOSFET gate voltage. To integrate an extraction gate with the cold cathode for a lower extraction bias is one of the possible solutions. In addition, from the typical I–V_{GS} curve obtained at V_A = 750 V (Fig. 4d), it is clear that the emission current can be precisely modulated by the V_{GS}. The emission current was regulated from 0.1 nA to 6.9 μA as the V_{GS} was increased from 0.812 V to 1.728 V in steps of 1 mV. It means that a large on/off current ratio of 2.3×10^5 was achieved by changing the V_{GS} over a very narrow range of 0.600–1.728 V. The on/off current ratio is much larger than that of a MOSFET-modulated ZnO-NWs cathode,[14] *i.e.* 5.6×10^3. We have found that the resistance of hydrothermally-grown ZnO-NWs fell in the range of 1.01×10^3–7.19×10^3 MΩ.[29] By contrast, the resistance of the GO film (1.14 MΩ–1.41 × 10^2 MΩ) is much lower than that of the ZnO-NWs. The two-terminal contact electrical measurements of the GO film and ZnO nanowires were performed in similar vacuum conditions by employing a nano-manipulated probe equipped with a SEM system, which makes the comparison reasonable. A large quantity of Joule heat was generated during the field emission. The ZnO NWs may be destroyed by the Joule heat from the high emission current. As a result, the maximum field emission current was relatively low and this limited the on/off current ratio of the MOSFET-modulated ZnO-NWs cathode.[14] Also, the GO film with two dimensional layouts may have a better heat dissipation performance.[30] Thus, a higher emission current (and thus a larger on/off current ratio) was achieved from the reduced GO cathode. Moreover, the on/off current ratio in the present work is larger than that of the TFT-modulated HfC-coated Si field emitter arrays, *i.e.* 1.0×10^4, even though a large emission current was achieved from the HfC-coated Si field emitter arrays.[31] We take the difference in the drain–source breakdown voltages ($V_{(BR)DSS}$) of the MOSFET and TFT into account for this phenomenon. The V_{DS} partly shares the anode bias during the MOSFET/TFT control measurement. The drain–source breakdown voltage of the MOSFET ($V_{(BR)DSS}$ = 400 V) is much higher than that of the TFT (several tens of volts). This allows the MOSFET to share more anode bias thus obtaining a larger on/off current ratio.

The field emission current stability of the MOSFET-control GO cathode was investigated at a constant V_A = 730 V. Here, we defined the current fluctuation to be $\sigma = |I - I_{ave}|_{max}/I_{ave}$, where I_{ave} is the average emission current intensity and $|I - I_{ave}|_{max}$ represents the absolute maximum between I and I_{ave} during the measurement. Initially, the V_{GS} was fixed at 2.000 V (the corresponding drain–source saturation current is 419.0 μA) and the I–t plot was recorded (the green line in Fig. 4e). In an 8-hour test, the current ranged over 3.4–8.3 μA. In this case, the channel of the MOSFET was "opened" and the field emission current was in an uncontrolled state. In this uncontrolled state, the fluctuation of the emission current is 57.4% (I_{ave} = 5.27 μA). Afterward, we reduced the V_{GS} until complete control of the emission current was achieved, *i.e.* V_{GS} = 1.703 V, as shown in Fig. 4e (the pink line). It is worth noting that the current fluctuation dramatically reduced to 3.4% (I_{ave} = 4.98 μA). This indicates that the stability of the emission current was remarkably improved, which benefits from the noise-buffer effect of the MOSFET channel. In addition, the I–t plots at a V_{GS} of 1.673 V (I_{ave} = 3.09 μA) and 1.596 V (I_{ave} = 1.04 μA) were also measured at V_A = 730 V. The current fluctuations are 6.4% and 19.9%, respectively. With a lower V_{GS}, the V_{DS} of the MOSFET shares more anode bias and the current saturation characteristics become poorer, resulting in a relatively high current fluctuation. We further applied the integrated GO cathode to a lab-prototype field emission display pixel demonstrating the active-control of the phosphor luminance. In order to get higher luminance, V_A was fixed at 800 V, even though a leakage current (I_{off} = ~1 nA) was observed at V_A = 800 V. Fig. 5 shows the typical luminance–V_{GS} curve and the corresponding images. The luminance of the pixel was modulated by the V_{GS}, ranging from 0.01 cd m^{-2} to 34.18 cd m^{-2} as the V_{GS} increased from 0.700 V to 1.720 V. At the high V_{GS} (1.735–1.940 V), the MOSFET channel is "open". The luminance is only dominated by V_A and shows a clear fluctuation, fitting well to the current stability test result. In addition, it is noted that the area of the luminance image (Fig. 5) is smaller than that of the GO films. We take the low anode voltage (800 V) and the non-uniformity of the field emission properties into account for explaining this observation. The brightness we obtained in the present work is 10 times lower than the general requirement (~300 cd m^{-2}) for commercial display applications. The low brightness is mainly due to the low anode voltage (800 V). The reason for employing a low anode voltage is to ensure the MOSFET works in a stable state. Nevertheless, the result confirms the feasibility of applying a MOSFET-modulated integrated cathode. For practical application, a low voltage phosphor is needed which is still a big challenge for the community. It may be easier to develop devices for close-eye display where only low brightness is required. The brightness can be improved by integrating the GO film with an extraction gate and further increasing the anode–cathode separation to endure a higher anode voltage. Further studies are needed.

4. Conclusions

A "vapor transportation" assembly technique was developed to attain layer-by-layer stacking continuous GO films for field electron emission applications. It was demonstrated that the GO films can be *in situ* reduced through a current conditioning, which can improve the conductivity and achieve an Ohmic contact at the GO–substrate interface. Enhanced field emission was obtained from the reduced GO films. GO films were locally deposited on the drain electrode of a MOSFET to obtain an integrated cathode. Actively modulation of both the field emission current and the phosphor luminance of a

lab-prototype display pixel were demonstrated. The work is meaningful to the applications of GO field emission cathodes for modern vacuum electronic devices.

Acknowledgements

This work was supported in part by the projects from the National Key Basic Research Program of China (Grant no. 2013CB933601), the National Natural Science Foundation of China (Grant no. 51290271, 51272293, 61222111), the Science and Technology Department of Guangdong Province, the Economic and Information Industry Commission of Guangdong Province, and the Science & Technology and Information Department of Guangzhou City, the projects from the Doctoral Fund of Ministry of Education of China (Grant no. 20120171110018).

References

1 X. Wang, L. J. Zhi and K. Müllen, *Nano Lett.*, 2008, **8**, 323.
2 D. Joung, A. Chunder, L. Zhai and S. I. Khondaker, *Nanotechnology*, 2010, **21**, 165202.
3 M. Qian, T. Feng, H. Ding, L. F. Lin, H. B. Li, Y. W. Chen and Z. Sun, *Nanotechnology*, 2009, **20**, 425702.
4 S. Stankovich, D. A. Dikin, R. D. Piner, K. A. Kohlhaas, A. Kleinhammes, Y. Jia, Y. Wu, S. T. Nguyen and R. S. Ruoff, *Carbon*, 2007, **45**, 1558.
5 A. T. T. Koh, Y. M. Foong, L. K. Pan, Z. Sun and D. H. C. Chua, *Appl. Phys. Lett.*, 2012, **101**, 183107.
6 D. Ye, S. Moussa, J. D. Ferguson, A. A. Baski and M. S. El-Shall, *Nano Lett.*, 2012, **12**, 1265.
7 Z. M. Xiao, J. C. She, S. Z. Deng, Z. K. Tang, Z. B. Li, J. M. Lu and N. S. Xu, *ACS Nano*, 2010, **4**, 6332.
8 H. Yamaguchi, K. Murakami, G. Eda, T. Fujita, P. F. Guan, W. C. Wang, C. Gong, J. Boisse, S. Miller, M. Acik, K. Cho, Y. J. Chabal, M. W. Chen, F. Wakaya, M. Takai and M. Chhowalla, *ACS Nano*, 2011, **5**, 4945.
9 Y. Huang, W. L. Wang, J. C. She, Z. B. Li and S. Z. Deng, *Carbon*, 2012, **50**, 2657.
10 J. C. She, S. Z. Deng, N. S. Xu, R. H. Yao and J. Chen, *Appl. Phys. Lett.*, 2006, **88**, 013112.
11 J. C. She, K. Zhao, S. Z. Deng, J. Chen and N. S. Xu, *Appl. Phys. Lett.*, 2005, **87**, 052105.
12 S. A. Guerrera, L. F. Velásquez-García and A. I. Akinwande, *IEEE Trans. Electron Devices*, 2012, **59**, 2524.
13 C. Li, Y. Zhang, M. T. Cole, S. G. Shivareddy, J. S. Barnard, W. Lei, B. P. Wang, D. Pribat, G. A. J. Amaratunga and W. I. Milne, *ACS Nano*, 2012, **6**, 3236.
14 W. J. Yang, J. C. She, S. Z. Deng and N. S. Xu, *IEEE Trans. Electron Devices*, 2012, **59**, 3641.
15 C. Mattevi, H. Kima and M. Chhowalla, *J. Mater. Chem.*, 2011, **21**, 3324.
16 C. Berger, Z. M. Song, X. B. Li, X. S. Wu, N. Brown, C. Naud, D. Mayou, T. Li, J. Hass, A. N. Marchenkov, E. H. Conrad, P. N. First and W. A. de Heer, *Science*, 2006, **312**, 1191.
17 W. Hummers and R. Offeman, *J. Am. Chem. Soc.*, 1958, **80**, 1339.
18 J. Kim, L. J. Cote, F. Kim, W. Yuan, K. R. Shull and J. X. Huang, *J. Am. Chem. Soc.*, 2010, **132**, 8180.
19 O. C. Compton and S. T. Nguyen, *Small*, 2010, **6**, 711.
20 C. Chen, Q. H. Yang, Y. Yang, W. Lv, Y. Wen, P. X. Hou, M. Z. Wang and H. M. Chen, *Adv. Mater.*, 2009, **21**, 3007.
21 R. Zacharia, H. Ulbricht and T. Hertel, *Phys. Rev. B: Condens. Matter Mater. Phys.*, 2004, **69**, 155406.
22 Y. J. Dappe, P. G. Bolcatto, J. Ortega and F. Flores, *J. Phys.: Condens. Matter*, 2012, **24**, 424208.
23 Y. J. Dappe, M. A. Basanta, F. Flores and J. Ortega, *Phys. Rev. B: Condens. Matter Mater. Phys.*, 2006, **74**, 205434.
24 J. Kang, D. Shin, S. Bae and B. H. Hong, *Nanoscale*, 2012, **4**, 5527.
25 Z. Q. Wei, D. B. Wang, S. Kim, S. Y. Kim, Y. K. Hu, M. K. Yakes, A. R. Laracuente, Z. T. Dai, S. R. Marder, C. Berger, W. P. King, W. A. de Heer, P. E. Sheehan and E. Riedo, *Science*, 2010, **328**, 1373.
26 K. Nakakubo, K. Asaka, H. Nakahara and Y. Saito, *Appl. Phys. Express*, 2012, **5**, 055101.
27 J. T. Chen, J. Li, J. Yang, X. B. Yan, B. K. Tay and Q. J. Xue, *Appl. Phys. Lett.*, 2011, **99**, 173104.
28 R. H. Fowler and L. Nordheim, *Proc. R. Soc. London, Ser. A*, 1928, **119**, 173.
29 H. He, J. C. She, Y. F. Huang, S. Z. Deng and N. S. Xu, *Nanoscale*, 2012, **4**, 2101.
30 K. L. Grosse, M. H. Bae, F. F. Lian, E. Pop and W. P. King, *Nat. Nanotechnol.*, 2011, **6**, 287.
31 M. Nagao, C. Yasumuro, Y. Sacho, H. Tanoue, S. Kanemaru and J. Itoh, *J. Vac. Sci. Technol., B: Microelectron. Nanometer Struct.–Process., Meas., Phenom.*, 2006, **24**, 936.